energies

MDPI

Article

Bidirectional Power Sharing for DC Microgrid Enabled by Dual Active Bridge DC-DC Converter

Sara J. Ríos [1], Daniel J. Pagano [2] and Kevin E. Lucas [1,2,*]

[1] Faculty of Electrical and Computer Engineering, ESPOL Polytechnic University, Campus Gustavo Galindo, Guayaquil 09-01-5863, Ecuador; srios@espol.edu.ec
[2] Department of Automation and Systems, Federal University of Santa Catarina (UFSC), Florianópolis 88040-900, Brazil; daniel.pagano@ufsc.br
* Correspondence: keveluca@espol.edu.ec

Abstract: Currently, high-performance power conversion requirements are of increasing interest in microgrid applications. In fact, isolated bidirectional dc-dc converters are widely used in modern dc distribution systems. The dual active bridge (DAB) dc-dc converter is identified as one of the most promising converter topology for the mentioned applications, due to its benefits of high power density, electrical isolation, bidirectional power flow, zero-voltage switching, and symmetrical structure. This study presents a power management control scheme in order to ensure the power balance of a dc microgrid in stand-alone operation, where the renewable energy source (RES) and the battery energy storage (BES) unit are interfaced by DAB converters. The power management algorithm, as introduced in this work, selects the proper operation of the RES system and BES system, based on load/generation power and state-of-charge of the battery conditions. Moreover, a nonlinear robust control strategy is proposed when the DAB converters are in voltage-mode-control in order to enhance the dynamic performance and robustness of the common dc-bus voltage, in addition to overcoming the instability problems that are caused by constant power loads and the dynamic interactions of power electronic converters. The simulation platform is developed in MATLAB/Simulink, where a photovoltaic system and battery system are selected as the typical RES and BES, respectively. Assessments on the performance of the proposed control scheme are conducted. Comparisons with the other control method are also provided.

Keywords: bidirectional power sharing; dc-dc converter; dc microgrid; dual active bridge (DAB); nonlinear control; robust control

Citation: Ríos, S.J.; Pagano, D.J.; Lucas, K.E. Bidirectional Power Sharing for DC Microgrid Enabled by Dual Active Bridge DC-DC Converte. *Energies* **2021**, *14*, 404. https://doi.org/10.3390/en14020404

Received: 2 November 2020
Accepted: 15 December 2020
Published: 13 January 2021

1. Introduction

In recent years, power electronic systems have been considered to be a solution for high efficiency power conversion systems, such as renewable power integration, energy storage interfaces, solid-state transformer, electric vehicles, and microgrids [1–6].

In fact, dc microgrids have become a more viable alternative solution for dc distribution system that is usually composed of multiple stages of power electronic converters [7,8]. DC microgrid is an attractive solution to integrate efficiently and suite better the renewable energy sources, energy storage systems, and loads at distribution or sub-transmission level. The DC microgrid is a locally controllable system that can operate either in grid-connected mode or stand-alone operation mode, i.e., completely isolated from the main transmission system [6,8,9].

The dc microgrid may overcome several drawbacks of ac systems, such as complexity of control for reactive power requirements, and lower system efficiency that is caused by a larger number of power conversion stages. Moreover, there are no frequency stability issues, harmonics issues, or skin effect in dc microgrid [9,10].

Despite the above advantages, the dc microgrids also face some challenges: (1) ensure power reliability; (2) overcome instability problems caused by constant power load

(CPL) behavior of point-of-load converter, and the dynamic interactions among multiple power converters; (3) integration into the conventional ac distribution grid; (4) ensure power balance among energy sources and loads; and, (5) achieve high-efficiency and high-performance power conversion.

Several control schemes have been introduced in order to ensure the proper operation of microgrid in grid-connected mode or stand-alone mode [11]. A comprehensive review on dc microgrids can be found in [12–14].

Research trends in power electronic converters have focused on improving the efficiency and power density, as well as reducing cost, volume, and weight.

Among dc-dc converters, isolated dc-dc converters are an attractive alternative for interfacing sources, such as photovoltaics, batteries, or fuel cells [6]. Therefore, there is an increasing requirement for bidirectional isolated dc-dc converters to ensure the power flow from, to, or between various energy storage elements.

The dual active bridge (DAB) dc-dc converter is identified as one of the most promising converter topology for the modern power electronic systems that require bidirectional power flow, galvanic isolation, and efficient power conversion.

DAB is an isolated bidirectional dc-dc converter composed of two full-bridge dc-ac converters interfaced by a series inductor and a high-frequency isolation transformer [15]. Figure 1 shows the circuit diagram of a DAB converter, where L is the DAB storage inductor; C_o is the dc output capacitor; a is the turns radio of the mediate/high-frequency transformer; v_i is the dc input voltage, while v_o is the dc output voltage; i_1 is the input current of the DAB input H-bridge; i_2 is the output current of the DAB output H-bridge; i_L is the DAB inductor current; and, i_o is the load current.

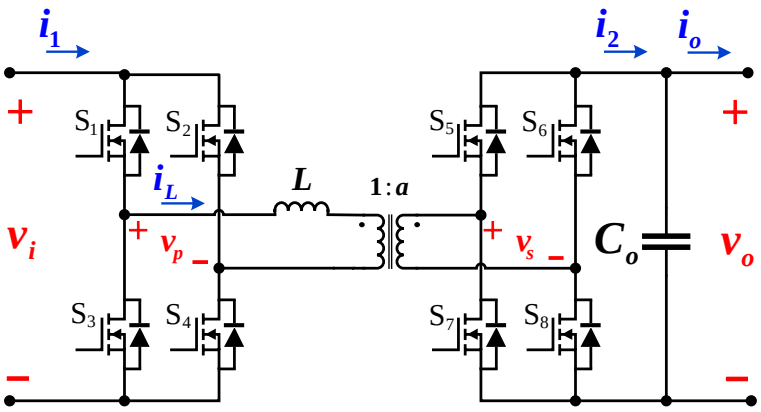

Figure 1. Circuit diagram of the dual active bridge (DAB) converter.

The basic mechanism for controlling the power flow is to generate two phase shifted high-frequency ac voltages (quasi-square or square wave) and applying them to the two ends of an energy-transfer inductor, thereby, energy flows from the leading ac voltage to the lagging ac voltage. Similar to power transmission control in traditional ac power systems, the power flow is controlled by the direction and magnitude of the inductor current i_L, which is changed by adjusting the phase shift between ac voltages (square-wave or quasi-square-wave) v_p and v_s of primary and secondary H-bridges, as shown in Figure 2. Thus, Figure 2 shows the simplified model for controlling the direction of power flow and magnitude of DAB converter.

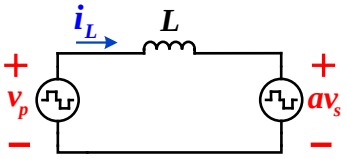

Figure 2. Lossless model, referred equivalent model of the primary side of the DAB dc-dc converter.

In general, a three-level ac voltage can be generated, where the duty-ratio can be adjusted by introducing an internal phase-shift between the two legs of the same H-bridge, as shown in Figure 3.

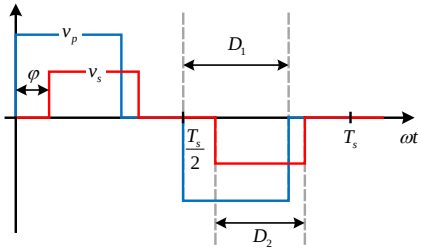

Figure 3. Primary (v_p) and secondary (v_s) transformer voltages for a specific modulation scheme.

Therefore, there are in total four degrees-of-freedom (DoF) to control the power flow of the DAB converter. Such DoF are composed of two internal phase-shift, corresponding to the primary bridge (D_1) and secondary bridge (D_2), respectively, an external phase-shift between two ac voltages (φ) and the switching frequency (f_s). In a DAB converter, and depending on the combination of these control parameters, some or all parameters, the modulation scheme can be classified into the following five categories: zingle-phase-shift (SPS) modulation [16], dual-phase-shift (DPS) modulation [17], extended-phase-shift (EPS) modulation [18], triple-phase-shift (TPS) modulation [19,20], and four-degrees-of-freedom (4DoF) modulation [21].

Although, the EPS, DPS, TPS, and 4DoF modulation schemes decrease the peak current and present a smaller back-flow power as compared to SPS modulation scheme, SPS is the main control strategy in real applications due to the convenience of control and easy implementation. In addition, the DAB converter can achieve an acceptable performance and efficiency under SPS modulation [22]. Therefore, this work adopts the SPS modulation scheme to control the DAB converter. Under the SPS modulation scheme, transformer saturation is a critical issue to deal with. To address this problem, the transformer saturation can be easily avoided as long as the parameter and structure of the high frequency transformer are properly designed while taking a constant frequency control scheme into account [23]. Therefore, the transformer is utilized to limit the fault current beyond the maximum value, i.e., zero power transfer (zero phase shift). Thus, the high-frequency transformer has to be designed for no load [24].

Under SPS control, power flow $\langle p(t)\rangle_{T_s}$ from the leading to lagging bridge can be defined as [15]:

$$\langle p(t)\rangle_{T_s} = \frac{\langle v_i(t)\rangle_{T_s}\langle v_o(t)\rangle_{T_s}}{2\pi a f_{sw} L_r}\varphi\left(1-\frac{|\varphi|}{\pi}\right) \quad (1)$$

where the phase-shift is φ, the switching frequency is f_{sw}, the switching period is $T_s = \frac{1}{f_{sw}}$, the average value of v_i in a switching period is $\langle v_i(t)\rangle_{T_s}$, and the average value of v_o in a switching period is $\langle v_o(t)\rangle_{T_s}$, all of the square waves whose duty cycle is 50 % are v_p and v_s, and the phase difference between them is φ $\left(-\frac{\pi}{2} \le \varphi \le \frac{\pi}{2}\right)$, when considering SPS control. Thus, If $\varphi > 0$, v_p gets ahead of v_s. Otherwise, v_p is lagging behind v_s [15,25].

In this context, the use of DAB dc-dc converter topology for dc microgrids offers some advantages over non-isolated dc–dc converters, such as soft-switching and galvanic isolation [15]. In addition, DAB converter has benefit characteristics, including bidirectional power flow capabilities, high efficiency, high power density, and buck/boost operation [15].

The benefits, drawbacks, and challenges of dc microgrids and distribution systems for different applications are well-described in [12,26,27], and the benefits, in the particular case of the DAB as interface in dc microgrids [28,29], can be summarized, as follows: (1) enhanced power density, efficiency, reliability, and modularity; (2) parallel connection of power sources does not require time-critical phase matching; and, (3) weight, size, and cost

reduction in magnetic components. Some research on dc systems that are enabled by DAB dc-dc converter may be found in [2,5,6,29–33].

According to the state-of-art discussed above, there are some advantage when the DAB converter is used in dc system applications. Therefore, this study addresses the operation and control of a dc microgrid in stand-alone operation, which is comprised of a PV generation system and a battery energy storage system (BESS), which are enabled with the common dc bus through DAB converters.

The aim of the BESS is to equalize the demand of generation and load by storing the excess energy of the PV system during light load conditions and releasing the energy during heavy load conditions. In order to address this challenge, a proposed power algorithm management is introduced to ensure the proper operation and the power balance in the islanded dc microgrid based on load/generation power and state-of-charge (SoC) of the battery conditions. Moreover, a nonlinear robust control is proposed for DAB converters in voltage-mode-control (VMC), aiming to enhance dynamic performance and robustness of dc-bus voltage.

The main contributions of this paper are briefly summarized, as follows:

- This study proposes a power management control strategy for PV and BESS systems with seamless mode transitions in order to ensure the power balance of a dc microgrid in stand-alone operation.
- In order to enhance the robustness of the dc-bus voltage, this work introduces an outstanding contribution for designing hybrid control structures when nonlinear systems are transformed into linear systems in order to overcome external disturbances, system uncertainties, and measurement noises. The proposed control scheme is based on the combination of Feedback Linearization Control (FLC) approach and robust parametric control approach.
- This study introduces a comprehensive point-of-view about the use of DAB converter in dc systems. In addition, an explanation to control the power flow in DAB dc-dc converter under SPS modulation scheme and the proposed power management control is also introduced.

The remainder of this paper is organized, as follows. Section 2 introduces the description of the dc microgrid. Section 3 addresses the operation and control of the dc microgrid in stand-alone operation. Section 4 describes the case studies to be performed in this paper. Section 5 summarizes the assessment of the simulation results. Finally, Section 6 presents the main conclusions.

2. Description of the DC Microgrid

DC MGs is usually composed of multi-stages of power conversion to integrate a variety of sources and loads, aiming at achieving the proper system operation [8]. Multi-stage power converter systems are known as cascaded power converter systems, where dc-dc converters are tightly regulated (point-of-load (POL) dc-dc converter) for voltage regulation and power conditioning. POL dc-dc converters exhibit a constant power load (CPL) behavior due to their regulation capability. CPL is a nonlinear load and introduces undesired oscillations into the dc-bus, which can degrade the stability margin or even destabilize the cascade system, although each stage is well-designed for stand-alone operation [8,9,34].

2.1. DC Microgrid Topology Motivation

In [6], a distributed power management strategy is introduced for a dc microgrid. The dc microgrid consists of renewable energy resources (fuel cell and photovoltaic panels) and energy storage device (battery), which share a common dc-bus through DAB dc-dc converter interface, in addition, a solid-state-transformer (SST), which is based on DAB converter topology, is used to interface the dc microgrid, the distribution system, and ac load. The authors in [2] claimed that DAB converter topology is suitable for photovoltaic (PV) applications, because it offers some advantages, such as multiport interface capability, high step-up ratio, wide input voltage range, and low input current ripple. Hence, a PV system that is

interfaced with a DAB converter achieves highly efficient maximum power point tracking (MPPT) and high reliability. In [35], a new control scheme is proposed for a medium-voltage photovoltaic-battery energy storage (PV-BES) system to overcome the power mismatch. DAB configuration enables independent MPPT, grounding of the PV generators, and ensures the the power balance with the batteries. In addition, the proposed power control configuration overcomes the small power mismatches without creating differential currents. In [31], the high performance and high efficiency of DAB converter for aerospace applications is analyzed and verified. The analysis is carried out in term of reliability, efficiency, volume, and weight for the specific application of a 270-V/28-V 10-kW bidirectional dc-dc converter. According to the state-of-art discussed above, this work adopts a dc microgrid, where the DAB converter enables the battery and PV system with the dc-bus to achieve high-performance power conversion requirements in microgrid applications.

2.2. Description of DC Microgrid Elements

Microgrid elements are briefly described below. Figure 4 shows a simplified dc microgrid with PV and battery energy storage systems, where the bidirectional DAB dc-dc converter is used in order to interface the battery with the dc-bus voltage to balance the power generated by the distributed energy resource (DER) and the load demand. As mentioned in Section 1, the PV generation system is enabled with the dc-bus through the DAB converter, where the power flow is unidirectional.

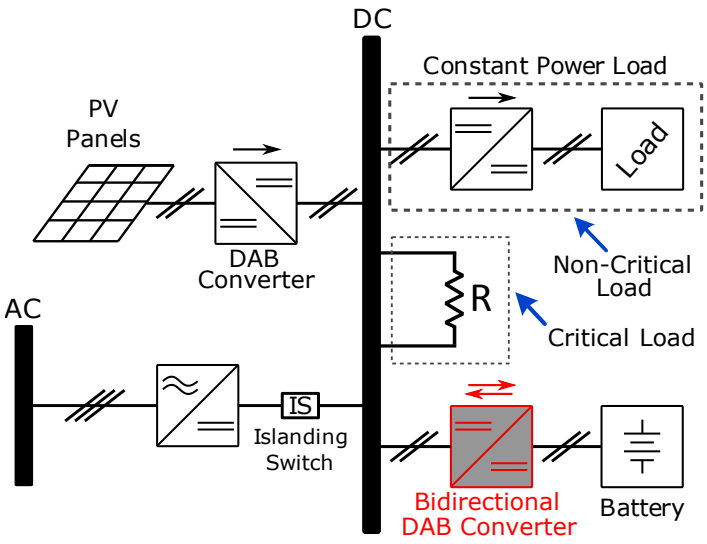

Figure 4. Simplified dc microgrid with a battery energy storage system.

When the dc MG is operating in islanded mode, only the DER and storage device provide the load power demand. Thus, it must provide reliable and flexible operation. In this context, the voltage stability of dc-bus can be ensured by balancing the power generated and load demand [36]. The power balance task is generally assigned to the battery energy storage devices connected into the dc-bus through a dc-dc bidirectional converter (cf. Figure 4). Hence, the BESS compensates the power fluctuation between the power generation side and load side.

The advantage of using the bidirectional dc-dc DAB converter topology is that it allows for isolating the battery from the dc-bus voltage. Thereby, if the battery suffers any issue, the voltage bus will not be affected. When there is excess of power generated, the BESS absorb that excess of available power in order to ensure the power balance, i.e., the bidirectional DAB converter operates in charging mode [36]. On the other hand, when the load demand exceeds the total power generated, the BESS supplies power to the dc MG in order to ensure the power balance, i.e., the bidirectional DAB converter operates in discharging mode [36]. Otherwise, the BESS remains floating or it is charged at a specific

rate. This rate is determined locally based on the battery SoC and the load/generation conditions [37].

Therefore, the bidirectional DAB converter of the BESS has two main goals when the dc MG is in stand-alone operation, i.e., isolated from the main grid: (i) handle bidirectional power flow in the battery; and, (ii) to keep regulated the dc-bus voltage, even driving nonlinear loads as CPLs [36]. The operation mode of the bidirectional DAB converter and nonlinear robust control design will be addressed in the next section.

The PV system (power generation) is composed of a DAB dc-dc converter (cf. Figure 4). The PV system operates with the a perturb and observes a MPPT algorithm. Thus, PV system may be modeled as a constant power source (CPS), i.e., injecting power into the common dc-bus.

The loads (cf. Figure 4) are comprised of a critical load as a resistance load (R), and a non-critical load as a dc-dc buck converter feeding a resistance load, with its output being regulated by a linear control system (PI controller). A single control loop is implemented in order to maintain the regulation of the output of the buck converter. The dc-dc DAB converter may be modeled as a CPL. Note that the non-critical load may be disconnected in order to ensure the power reliability of the dc microgrid.

Figure 5 shows the overall equivalent microgrid circuit in stand-alone operation, where P_{pv} and P_{CPL} represent the total power of the PV system and CPL, respectively. In addition, the power consumed by the resistance load (R) is represented by P_R, while the battery power and the maximum battery power are defined by P_{Bat} and P_{Bat}^{max}, respectively.

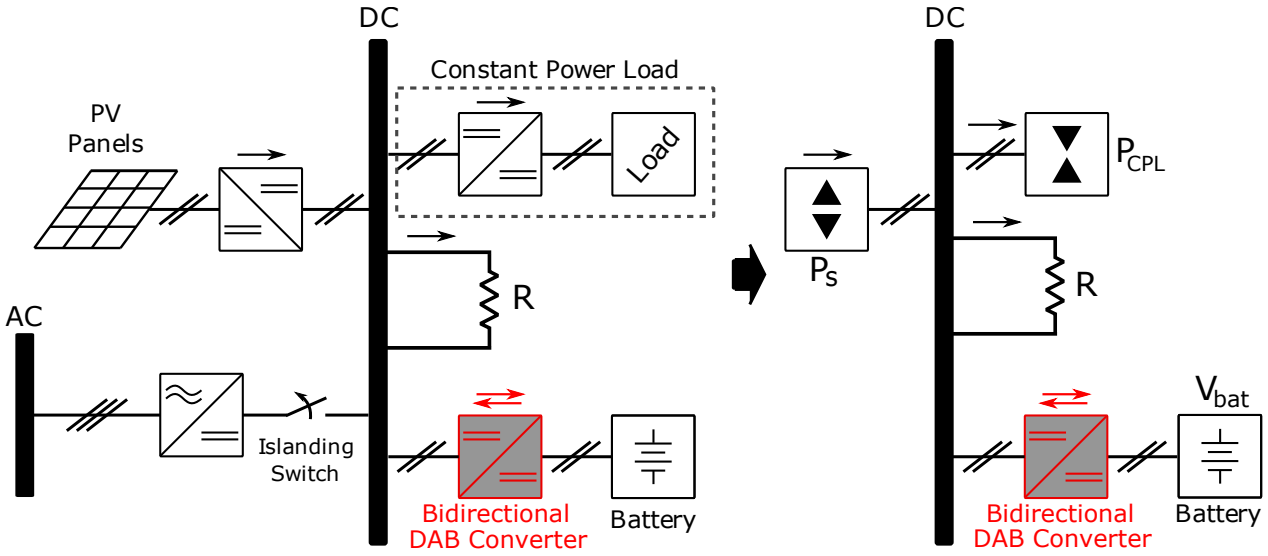

Figure 5. Microgrid equivalent (reduced) model.

3. Operation and Control of DC Microgrid in Stand-Alone Operation

The main challenge is ensure the power reliability of the dc microgrid in stand-alone operation. The power unbalance among energy sources and loads is one of the main challenges, because it affects the reliability in a DC MG. Thus, in this section, a power management control algorithm, operation mode, and local controllers of DAB converters are introduced, aiming at ensuring a proper operation of the dc microgrid.

3.1. Power Management Algorithm

Power management and bus voltage control of microgrid systems can be a complicated task, since, for instance, the PV power output will change as the irradiance changes; the load is not always constant; DER and BESS have different dynamic responses, to name a few. Therefore, in order to supply reliable and high quality energy to users, the power management system should consider these factors [6].

In stand-alone PV applications, BESS is usually implemented to balance generation with load, thus allowing for the photovoltaic converter to regulate the load voltage [38].

The power balance issue in the presence of a PV system is more challenging in dc MGs in stand-alone operation for several reasons. First, the storage device may be installed, without direct control interconnection with the PV unit, as a separate unit in a different location in the dc microgrid. Second, the PV unit is generally controlled as a current-controlled source mode to inject all available power into the DC microgrid. This strategy was first introduced for grid-connected applications, where the power balance between generation and load is maintained through the main grid. Finally, dc MG is plug and play, i.e., may introduce other units with different control strategies that must be considered for the design of the power management control scheme [38]. Hence, the operation of the PV unit and battery storage unit must be coordinated with that of other units in the islanding microgrid to maintain power balance, when considering the SoC limits of the battery storage to avoid significant battery lifetime deterioration due to being undercharged or overcharged.

In this paper, the power management algorithm controls the operation mode of PV system and BESS, in addition to disconnecting/connecting the PV generation system or the non-critical load aiming at ensuring the power balance of the dc microgrid. Battery operating mode is determined based on its SoC; hence, the Battery SoC must be taken into account in the power management algorithm. Moreover, the battery system has three basic modes due to its the bidirectional power flow nature: (i) battery discharging mode; (ii) battery charging mode; and, (iii) battery standby mode (SoC out of limit). In this context, the battery operation must seamlessly switch among three operation modes, depending on the power conditions of the dc microgrid.

In the battery discharging mode, the DAB converter of BESS regulates the dc-bus voltage (v_{dc}), while, in the battery charging mode, it controls the current to charge the battery. Thus, there is a issue to solve when the BESS is in battery charging mode, because other sources must regulate the dc-bus voltage. For the dc microgrid under study (cf. Figure 5), only the PV system may carry out such a task. Under normal conditions, PV system provides the maximum available power of the photovoltaic panels, but in this critical situation, this power converter must change its mode of operation MPPT for voltage source [39–41]. Because this microgrid under study does not have a communication link between its elements, the power management algorithm can select the operation mode of the DAB converter of the PV system, Thereby, the PV system operates in voltage source (VMC) or MPPT mode.

Figure 6 shows the operation mode of PV system and BESS, depending on the power management algorithm. Figure 6 also presents the control-loop diagram for each operation mode.

In order to select the proper operation mode (cf. Figure 6), a decentralized scheme is introduced called power management algorithm, which depends on load/generation powers and the battery SoC.

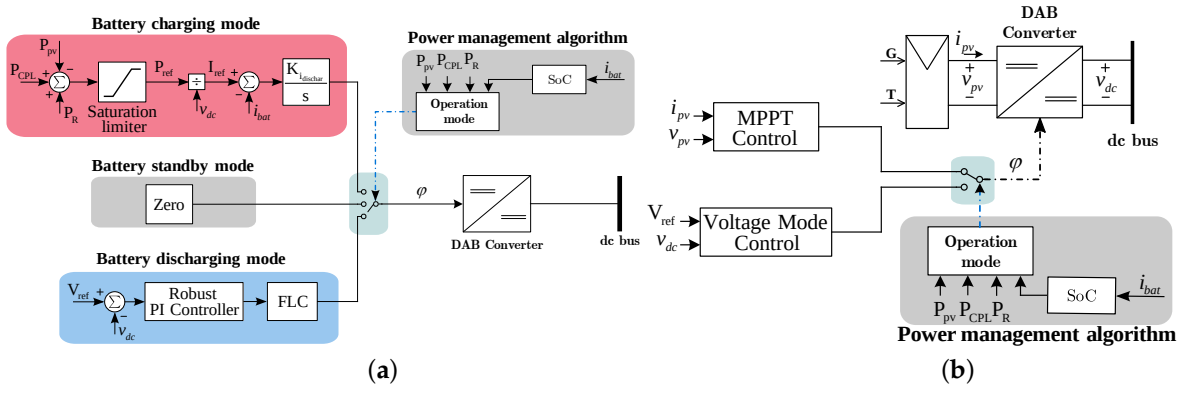

Figure 6. Control schemes for BESS and PV system. (**a**) battery energy storage system; (**b**) PV system.

Thereby, two levels may be defined based on the SoC of the battery, since the SoC cannot be upper than a threshold to avoid significant damages in the battery life due to the depth of discharge and excessive charge.

In this paper, an upper level $\mathrm{SoC_{upper}} = 90\%$ and a lower one $\mathrm{SoC_{lower}} = 40\%$ are defined. For $\mathrm{SoC} < \mathrm{SoC_{lower}}$, the dc-dc power converter must operate in battery charging mode. For $\mathrm{SoC} > \mathrm{SoC_{upper}}$, the dc-dc power converter must operate as a battery standby mode and stop absorbing power, because the battery unit is almost fully charged, unless the generated power is less than loads need; more details will be described later. Otherwise, both operation modes (charging or discharging) may be selected, depending on the load/generation conditions of the dc microgrid.

The SoC of the battery [42] is given by

$$\mathrm{SoC}(t) = \mathrm{SoC}(t_o) - \frac{1}{c_n}\int_{t_o}^{t} i_{bat}\,dt \tag{2}$$

where $\mathrm{SoC}(t_o)$ is the initial SoC estimation and c_n is the battery capacity. Due to the time constant of the battery being slow, its dynamic can be neglected [39].

Since the bidirectional DAB dc-dc converter connects the BESS into the dc-bus voltage, the power flow direction depends on the operation mode (cf. Figure 6). Due to SPS control, $\varphi > 0$ is considered for battery discharging mode and $\varphi < 0$ for battery charging mode. When $\varphi = 0$, the power is zero.

Figure 7 illustrates a flowchart of the proposed power management algorithm in order to select the operation mode of both PV system and BESS, aiming at ensuring the power balance of the dc microgrid in stand-alone operation. It is important that the proposed power management algorithm only requires local information. Table 1 describes the states and actions that decide the operation of the dc microgrid in stand-alone operation, where ST1, ST2, and ST3 are the states that select the proper operation mode of PV system and BESS, while AC1 and AC2 handle disconnection (if their values are equal to zero) or reconnection (if their values are equal to one) of non-critical load and PV generation system, respectively, and the state OFF disconnects the dc microgrid. Note that $\mathrm{P_L}$ is the sum of the powers of the loads ($\mathrm{P_L} = \mathrm{P_R} + \mathrm{P_{CPL}}$).

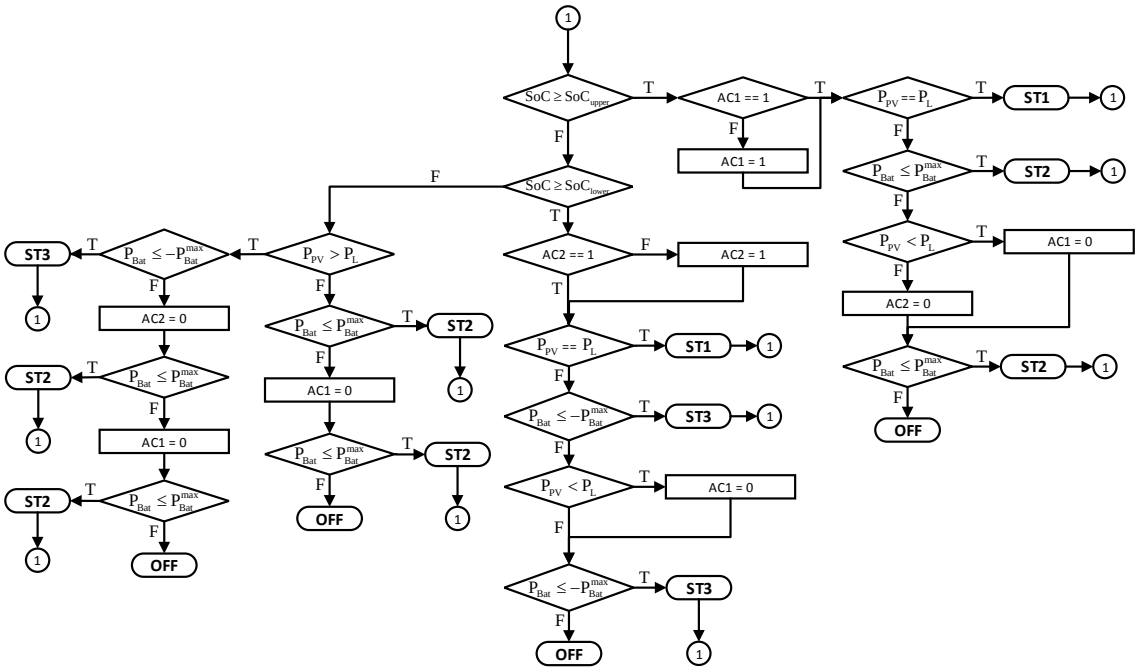

Figure 7. Flowchart of the proposed power management algorithm.

Table 1. Description of states and actions of the power management algorithm.

States	Description
ST1	This state selects the **battery standby mode** of BESS and **voltage mode control** of the PV system
ST2	This state selects the **battery discharging mode** BESS and of **MPPT mode** of the PV system
ST3	This state selects the **battery charging mode** of BESS and **voltage mode control** of the PV system
AC1	This variable handles **disconnection** and **reconnection** of the non-critical load
AC2	This variable handles **disconnection** and **reconnection** of the PV generation system

3.2. Battery Discharging Mode Control

According to the proposed control scheme (cf. Figure 6), in this operation mode, the DAB dc-dc converter with the battery unit regulates the microgrid common dc-bus voltage. Thus, the DAB converter is set to voltage-mode control in order to regulate the dc-bus voltage (v_{dc}).

The dc microgrid net power may be modeled as $P = Ps + P_{CPL}$, which results in a simplified model, as shown in Figure 8. Thus, the bidirectional DAB dc-dc converter plays the role of maintaining the power balance, depending on load/generation conditions, while using the battery to supply power to the MG or drain power from it.

Figure 8 illustrates the proposed control scheme for the DAB dc-dc converter in battery discharging operation mode.

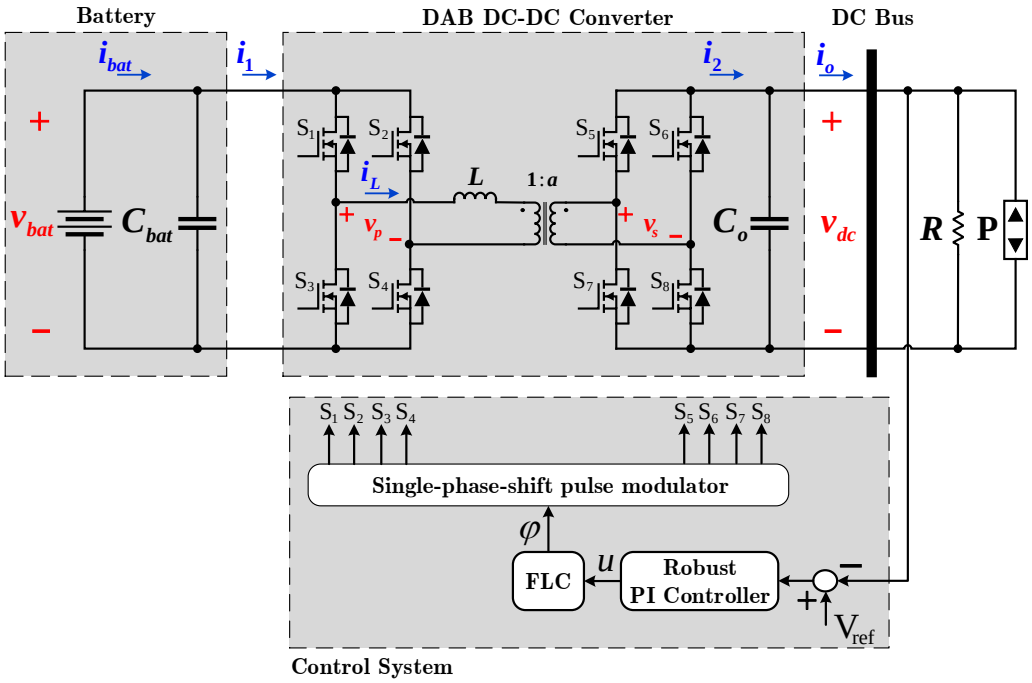

Figure 8. Proposed control scheme for DAB converter in battery discharging mode under single-phase-shift (SPS) modulation.

From Kirchhoff's current law at the DAB output terminal, the equation representing the variation of the average value of v_o is defined.

$$C_o \frac{d\langle v_{dc}(t)\rangle_{T_s}}{dt} = \langle i_2(t)\rangle_{T_s} - \langle i_o(t)\rangle_{T_s} \tag{3}$$

The power losses are not considered in this model. thus, the secondary side dc current is defined from the power balance equation [25,43], as follows:

$$\langle p(t)\rangle_{T_s} = \langle i_2(t)\rangle_{T_s}\langle v_{dc}(t)\rangle_{T_s}$$

$$\Rightarrow \langle i_2(t)\rangle_{T_s} = \frac{\langle v_{bat}(t)\rangle_{T_s}}{2\pi a f_{sw} L_r}\varphi\left(1 - \frac{|\varphi|}{\pi}\right) \tag{4}$$

The following variables are defined in order to simplify the analysis [25]

$$\omega_{sw} = 2\pi f_{sw} \ , \ g_m = \frac{1}{\pi a \omega_{sw} L_r} \tag{5}$$

Substituting (4) and (5) into (3), and assuming that $\varphi > 0$,

$$C_o \frac{d\langle v_{dc}(t)\rangle_{T_s}}{dt} = g_m \langle v_{bat}(t)\rangle_{T_s}\varphi(\pi - \varphi) - \langle i_o(t)\rangle_{T_s} \tag{6}$$

with

$$i_o = \underbrace{\frac{v_{dc}}{R}}_{i_R} + \underbrace{\frac{P}{v_{dc}}}_{i_P} \quad \text{and} \quad P = \mathrm{P_{PV}} + \mathrm{P_{CPL}}$$

The control objective is that the dc-bus voltage (v_{dc}) remains regulated at the operating point that is defined by $\mathrm{V_{ref}}$, even under large disturbances. Because CPL introduces non-linearity into the system, classical linear controllers are not sufficient for mitigating oscillations effects and ensuring system stability under large signal disturbances. Therefore, we propose the combination of FLC and robust control methodologies for designing fixed order nonlinear robust controller (cf. Figure 8) [43].

First, the CPL linearization is performed in order to overcome the non-linearity that is introduced by a CPL. Second, the resulting equation is transformed into a linear equation while using FLC. Finally, the robust controller design is introduced.

3.2.1. CPL Linearization

We assume the worst case for the controller design, i.e., when there is no power generation by the source, $\mathrm{P_{PV}} = 0$, yielding Equation (7).

Because the simplified model of CPL is nonlinear, the linearization around an voltage operating point V_{dc} is usually performed. Note that V_{dc} and $\mathrm{P_{CPL}}$ represent the dc value (operating points) [8,43].

$$i_{CPL} \approx 2\frac{\mathrm{P_{CPL}}}{V_{dc}} - \frac{\mathrm{P_{CPL}}}{V_{dc}^2} v_{dc} \ , \ R_{\mathrm{CPL}} = -\frac{V_{dc}^2}{\mathrm{P_{CPL}}} \tag{7}$$

The linearization of CPL yields the the following nonlinear Equation (8), where the CPL is linearized around the operating point.

$$C_o \frac{d\langle v_{dc}(t)\rangle_{T_s}}{dt} = g_m \langle v_{bat}(t)\rangle_{T_s}\varphi(\pi - \varphi) - \frac{1}{R_{eq}}\langle v_{dc}(t)\rangle_{T_s} \tag{8}$$

where,

$$R_{eq} = R \,||\, R_{\mathrm{CPL}}$$

3.2.2. Feedback Linearization Control

The average model for the DAB converter with Linearized CPL (8) is a nonlinear continuous-time equation due to the cross-product between phase-shift (φ) and and the square of φ with the averaged battery voltage of v_{bat}. Note that the non-linearity that is introduced by the CPL $\left(\mathrm{P_{CPL}}/\langle v_{dc}(t)\rangle_{T_s}\right)$ does not take into account the feedback linearization controller design, since the instantaneous value of P_{CPL} is unknown.

The voltage control loop is designed based on the FLC technique in order to transform a nonlinear system into a linear system, overcoming the non-linearity (8).

When considering the dynamic Equation (8), where $\langle v_{dc}(t)\rangle_{T_s}$ is the system output and φ is the control signal, let $u(t)$ be a new auxiliary input variable

$$u(t) = V_{bat}\varphi(\pi - \varphi) \tag{9}$$

to describe a new linear relationship (10) that represents the dynamics of the output voltage v_{dc}. Note that $\langle v_{bat}(t)\rangle_{T_s} = V_{bat}$

$$C_o\frac{d\langle v_{dc}(t)\rangle_{T_s}}{dt} = g_m u(t) - \frac{1}{R_{eq}}\langle v_{dc}(t)\rangle_{T_s} \tag{10}$$

Therefore, the small-signal control-to-output transfer function of the DAB converter with FLC is

$$G_{vd}(s) = \frac{v_{dc}(s)}{u(s)} = \frac{g_m}{C_o}\left(\frac{1}{s + \frac{1}{C_o R_{eq}}}\right) \tag{11}$$

In order to meet the closed-loop performance requirements, a linear controller may be designed based on (11). Note that R_{eq} varies when $\mathrm{P_{CPL}}$ or R change. This involves using a robust control design [7,44], as will be seen below.

3.2.3. Robust Control Design

A PI controller structure (12) is adopted as the voltage controller to regulate the dc-bus voltage v_{dc}.

$$C_1(s) = \frac{K_p s + K_i}{s} \tag{12}$$

The controller is designed according to [9,43], which leads to a set of linear inequality constraints. This control technique is successfully employed in [25,43] to control a DAB converter under parametric uncertainties and CPL variation, respectively.

Hence, a region of uncertainty is previously defined in order to design robust controllers. Thereby, the resistance load variations (ΔR) and CPL power variation ($\Delta\mathrm{P_{CPL}}$) are defined as the system uncertainties.

$$\begin{cases} \Delta\mathrm{R} = [R^{\min},\ R^{\max}] \\ \Delta\mathrm{P} = [\mathrm{P}_{\mathrm{CPL}}^{\min},\ \mathrm{P}_{\mathrm{CPL}}^{\max}] \end{cases} \tag{13}$$

Thus, a box region in plant parameters is built from the system uncertainties, which results in an interval plant model (14).

$$G_{vd}(s) = \frac{v_{dc}(s)}{u(s)} = \frac{g_m}{C_o}\left(\frac{1}{s + \frac{1}{C_o \Delta \mathrm{R_{eq}}}}\right) \tag{14}$$

Note that $\Delta\mathrm{R_e q}$ is calculated as follows:

$$\Delta\mathrm{R_{eq}} = \Delta\mathrm{R}\ ||\ \Delta\mathrm{R_{CPL}},\ \mathrm{R_{CPL}} = -\frac{\mathrm{V_{dc}}^2}{\Delta\mathrm{P_{CPL}}}$$

For simplification, the interval transfer functions (14) is be represented, as follows:

$$G_{vd}(s) = \frac{b_0}{s + [a_0]} \tag{15}$$

Because G_{vd} is an interval plant, its corresponding closed-loop characteristic polynomial will be a closed-loop characteristic interval polynomials (16),

$$\Phi(s) = [\Delta^{\min}, \Delta^{\max}] = s^2 + [\gamma_1]s + [\gamma_0] \tag{16}$$

where:

$$[\gamma_0] = b_0 K_i$$
$$[\gamma_1] = [a_0] + [b_0] K_p$$

The desired closed-loop polynomial is represented below:

$$\Delta_d(s) = s^2 + 2\xi\omega_n s + \omega_n^2 = s^2 + \phi_1 s + \phi_0 \tag{17}$$

The closed-loop polynomial parameters (16) are compared with the desired closed-loop polynomial (17) in order to tune the controller parameters. This comparison may be rewritten in its matrix format, resulting in the following relationship (18).

$$\underbrace{\begin{bmatrix} b_0 & 0 \\ 0 & b_0 \end{bmatrix}}_{A} \underbrace{\begin{bmatrix} K_p \\ K_i \end{bmatrix}}_{X} = \underbrace{\begin{bmatrix} \phi_1 - [a_1] \\ \phi_0 \end{bmatrix}}_{B} \tag{18}$$

When parametric uncertainties disturb the system, the controller performance can degrade. Hence, the controller must ensure robust performance. Thus, the controller must ensure system stability and robust performance within the region of uncertainties where the system parameters vary. Therefore, a desired region is defined below:

$$\Delta_d := \{\phi_i^{\min} \leq \phi_i \leq \phi_i^{\max}\} \tag{19}$$

Therefore, according to [9,25,34,43], It is possible to formulate a set of linear inequalities (20) that restricts the desired polynomial coefficients and the controller parameters in the predefined intervals.

$$\begin{bmatrix} \phi_1^{\min} - [a_1] \\ \phi_0^{\min} \end{bmatrix} \leq \begin{bmatrix} b_0 & 0 \\ 0 & b_0 \end{bmatrix} \begin{bmatrix} K_p \\ K_i \end{bmatrix} \leq \begin{bmatrix} \phi_1^{\max} - [a_1] \\ \phi_0^{\max} \end{bmatrix} \tag{20}$$

Thus, Equation (20) can be rewritten as

$$B(\phi^{\min}) \leq AX \leq B(\phi^{\max}) \tag{21}$$

The choice of $K = [K_p \quad K_i]^T$ (if possible) solves the robust control design problem, satisfying the set of inequality (20). The solution of this problem may be addressed as a solution to a linear programming problem. Thus, this problem (20) may be rewritten as a local minimization problem, subject to restrictions according to [9].

The robust control design problem is summarized in the choice of $K = [K_p \quad K_i]^T$ (if possible) to satisfy the set of inequality (20). The solution of this problem can be idealized, as a solution to a linear programming problem. Therefore, this problem (20) can be rewritten as a problem of local minimization, which is subject to restrictions according to [9].

$$\begin{aligned} &K_a = \arg(\min f(X_a)) \\ &s.t. \begin{bmatrix} A_a \\ -A_a \end{bmatrix} K_a \leq \begin{bmatrix} B(\phi^{\max}) \\ -B(\phi^{\min}) \\ 0 \end{bmatrix} \end{aligned} \tag{22}$$

with

$$X_a = \begin{bmatrix} X \\ R \end{bmatrix}, A_a = \begin{bmatrix} A & \|a\|_2 \\ -A & \|a\|_2 \\ 0_{1\times 2} & -1 \end{bmatrix} \tag{23}$$

where the cost function is defined as the sum of controller gains within the radio R; $\|a\|_2$ is the euclidean norm of coefficients of A; where, $\|a\|_2$ is the euclidean norm of coefficients of A; the cost function is defined as the sum of controller gains within the radio R; and, the parameter vector X_a contains the controller gains and the radio R, which means R stands the radio of the largest ball of Chebyshev Theorem. Note that Chebyshev Theorem takes the polytope with the larger uncertainty of the systems into account (power load conditions).

The feasible solution is then implemented to set the controller structure (13). The discrete equivalent of the designed controller is obtained through the Tustin method while using a sampling rate of $T_s = 1/f_{sw}$.

Finally, the control parameter value φ actually sent to the SPS pulse modulator is defined by,

$$\varphi = \frac{\pi - \sqrt{\pi^2 - \frac{4u(t)}{V_{bat}}}}{2} \tag{24}$$

where, $\pi^2 - \frac{4u(t)}{V_{bat}} > 0$, and the solution for φ is the negative root, since φ is defined in the control design to operate from 0 to $\frac{\pi}{2}$.

3.3. Battery Charging Mode Control

When DAB dc-dc converter operates in battery charging mode, other sources must regulate the common dc-bus voltage [39–41]. As mentioned in Section 3.1, the PV system will be operate in voltage mode control maintain regulated the dc bus when the BESS is in battery discharging mode (cf. Figures 6 and 7). Thus, the VMC of the PV is the same VMC for the BESS; hence, the same controller scheme used for battery discharging mode (cf. Figure 8) will be used in the PV system.

The battery charger control using a bidirectional DAB dc-dc converter is proposed in Figure 4, where $\varphi < 0$ for this operation mode. A desired Power, $\mathrm{P_{ref}}$, is generated while using a the following relationship:

$$\mathrm{P_{ref}} = \mathrm{P_R} + \mathrm{P_{CPL}} - \mathrm{P_{pv}} \tag{25}$$

note that $\mathrm{P_{ref}}$ is saturates between upper and lower limits, i.e., it operates between zero and the maximum discharge power allowed given by $(-\mathrm{P_{Bat}})$. Subsequently, the desired power, $\mathrm{P_{ref}}$, is divided for the measured dc bus voltage, v_{dc}, in order to determine the reference current,

$$\mathrm{I_{ref}} = \frac{\mathrm{P_{ref}}}{v_{dc}} \tag{26}$$

Finally, an integral controller (26) is used to ensure zero-steady-state error and determine the control parameter value φ actually sent to the SPS pulse modulator.

$$C_{Char}(s) = \frac{\mathrm{K_{i_{Dichar}}}}{s} \tag{27}$$

4. Description of Case Studies

Table 2 presents the dc microgrid parameters and the meaning of each symbol.

Simulations are performed when considering well-designed DAB converter parameters taking account magnetic components; output, and coupling capacitors; switching devices to avoid the transformer saturation, obtain the desired voltage ripple, and overcome current and voltage stress in switching components, respectively. Moreover, the dc microgrid has been simulated while using MATLAB® with the toolbox SimPowerSystems™. The power converter switching models and the discrete-version of the control

laws have been implemented in MATLAB® to perform simulations as similar to real tests. In addition, a fictitious battery with a very low capacity is considered, since its dynamic is too slow and the power converter switching models are considered.

This study aims to show the effectiveness of the proposed power management algorithm that is based on the battery SoC and instantaneous powers (cf. Figure 7) to select the proper operation mode of DAB dc-dc converters in order to ensure the power balance of a dc microgrid in stand-alone operation. The robustness of the proposed nonlinear controller enhances the dc-bus voltage dynamic performance and it is compared to a classical controller. Table 3 summarizes each controller gain.

In order to design the controllers, the following (nominal) requirements are chosen to regulate the DAB converters when they are in VMC: settling time $t_{set} \leq 30$ ms and damping factor $\xi \geq 0.69$. It is worth mentioning that the same design parameters are used for both controllers. More details for the control design are summarized in [43]. In this work, several control techniques are addressed, including the robust FLC approach in detail for a DAB converter feeding a CPL.

Table 2. Microgrid Parameters.

Parameter	Symbol	Value
Battery energy storage system		
Battery voltage	V_{bat}	400 V
DC-bus voltage	v_{dc}	400 V
Phase-shift at rated power	φ	45^0
Series inductance	L	125 µH
Inductor resistance	r_L	70 mΩ
Coupling capacitor	C_b	20 µF
Output Capacitor	C_o	470 µF
Transformer turns ratio	a	1
Switching frequency	f_{sw_1}	40 kHz
Output Power	P_{bat}	3 kW
PV System with DAB Converter		
PV Power	P_v	3 kW
Series inductance	L_1	125 µH
Inductor resistance	r_{L1}	70 mΩ
Coupling capacitor	C_{b1}	20 µF
Output Capacitor	C_2	470 µF
Transformer turns ratio	a	1
Switching frequency	f_{sw_2}	40 kHz
Buck Converter		
Maximum output Power	P_o	3 kW
Switching frequency	f_s	40 kHz
Input voltage	V_{dc}	400 V
Filter inductor	L_2	100 µH
Output Capacitor	C_2	4700 µF
Resistance Load		
Load resistance	R	53.33 Ω

In this context, three case studies are performed in order to evaluate the proposed bidirectional power sharing of dc microgrid that is enabled by DAB dc-dc converters. A brief description of case studies are summarized in the following subsections.

Table 3. Designed controllers for DAB converter.

DAB in Voltage Mode Control		
	K_p	K_i
Classical Control	0.00296	0.01990
Robust FLC	5.57139	623.561
DAB in Current Mode Control		
$K_{i_{Dichar}}$	3.0	

4.1. Case Study I: Disconnection of the Generation Source

This case study aims to illustrate the power balance of the dc MG, depending on the generation/load power variations based on the proposed power management algorithm. The power management algorithm (cf. Figure 7) identifies the appropriate operation mode of the battery energy storage system (charging, discharging, or standby mode) and the PV generation system (MPPT or VMC mode), as depicted in Figure 6a,b, respectively. When the BESS operates in charging mode and the SoC of battery achieves its upper limit ($SoC_{upper} = 90\%$), the DAB converter needs to change the operation mode of the BESS. This test assumes that the power that is generated by PV system is greater than powers that are consumed by the loads, i.e., $P_{PV} > P_R + P_{CPL}$, when the above mentioned change of operating mode occurs. Thereby, the generation source (PV system) will be disconnected and the BESS will supply power to loads (battery discharging mode), provided that its maximum power is greater than the powers that ae consumed by the loads, i.e., $P_{Bat} \geq P_R + P_{CPL}$; otherwise, the non-critical load will be disconnected. Moreover, dynamic performance of the dc-bus voltage is compared when the dc-bus is regulated by the classical and proposed controllers.

4.2. Case Study II: Disconnection of the Non-Critical Load

The aim of the second test is to evaluate the power balance of the dc MG according to the power management algorithm (cf. Figure 7). The non-critical load will be disconnected in two cases: (i) for battery discharging mode, if the sum of the powers of BESS and PV system is lower than loads need; (ii) for battery charging mode, if the power that is generated by PV system is not larger than loads need. In this case, the second case is illustrated. In addition, the oscillations into the dc-bus voltage are also analyzed under the classical and proposed control approaches.

4.3. Case Study III: DC Bus Voltage Regulation Capability

The last case is performed in order to evaluate the dc-bus voltage regulation capability when the DAB converter of the BESS operates in battery discharging mode. The power management conditions are set by the power management algorithm (cf. Figure 7). The oscillation of the dc-bus voltage is analyzed under different load/generation power conditions. In order to prove the robustness and effectiveness of the proposed controller, it is compared to a classical controller.

5. Assessment of Results

5.1. Case Study I: Disconnection of the Generation Source

The simulation results for the case study I are shown in Figures 9 and 10, where Figures 9a,b and 10a,b represent the dc-bus voltage, instantaneous powers of the dc MG, the SoC of the battery, and the phase-shift control signal, and the pulse voltage of primary v_p and secondary v_s full-bridges, respectively, under different load/generation power conditions.

The PV power (P_{PV}) is set in 3000-W and the battery is assumed to be fully charged with a SoC of the battery of 90% at the beginning of the simulation. For this case, the dc MG starts with the PV system feeding the loads (resistance load and CPL), because the

generation power is equal to the power that loads need, thereby, the BESS operates in battery standby mode, i.e., the battery power is zero ($P_{Bat} = 0$) in order to maintain the power balance in the dc MG. Therefore, there is no phase-shift between the pulse voltage of the primary (v_p) and secondary (v_s) full-bridges, as shown in Figure 10b.

During $0.4 < t < 0.8$ s, the CPL power increases from 1000-W to 3000-W; thus, the power of the loads ($P_R + P_{CPL} = 5000$-W) is larger than the PV power ($P_{PV} = 3000$-W); hence, the power management algorithm identifies a change in the operation mode; thus, the DAB converter of the BESS changes its operation mode from battery standby mode to battery discharging mode, regulating the common dc-bus voltage. When the BESS is in battery discharging mode, the phase-shift (φ) must be between $\left(0, \frac{\pi}{2}\right)$ (cf. Figure 10a); thus, the pulse voltage of the primary full-bridge (v_p) gets ahead of the pulse voltage of the secondary full-bridge (v_s) (cf. Figure 10b).

The BESS will continue to operate in battery discharging mode until any load/ generation condition occurs or its lower battery SoC limit ($SoC_{lower} = 40\%$) is reached. At time $t = 0.8$ s, the powers that are consumed by loads decrease ($P_R = P_{CPL} = 1000$-W)); as a result, the PV power ($P_{PV} = 3000$-W) is larger than loads needs ($P_R + P_{CPL} = 2000$-W); thus, the battery absorbs the extra power from the PV system, thereby, the BESS starts operating in battery charging mode (cf. Figure 9b). When this occurs, the dc-bus voltage is regulated by the DAB converter of the PV system, i.e., it operates in voltage mode control, as discussed in Section 3 (cf. Figure 6b). This transition between operation modes is performed by the power management algorithm. When the BESS operates in battery charging mode, the phase-shift (φ) must be between $\left(-\frac{\pi}{2}, 0\right)$; thus, the pulse voltage of the primary full-bridge (v_p) is lagging behind the pulse voltage of the secondary full-bridge (v_s), as shown in Figure 10b.

The BESS will continue to operate in battery charging mode until the generation power is larger than loads need or the upper battery SoC limit ($SoC_{upper} = 90\%$) is reached. In this context, the lower battery SoC limit is reached at $t \approx 1.76$ s, as shown in Figure 10a; thus, the BESS will change its operation mode to battery standby mode if the power generation is equal to the power that loads need ($P_{PV} = P_R + P_{CPL}$), or battery discharging mode if the power consumption by load is greater than generation power ($P_{PV} < P_R + P_{CPL}$); otherwise, the power generation system (PV system) will be disconnected, and the BESS will supply energy to loads, more details about the operation mode and power management in Figure 7. According to Figure 9a, when the battery SoC reaches its upper limit ($SoC_{upper} = 90\%$), the generation power is larger than loads need; hence, the PV system is disconnected and the BESS starts to operate in battery discharging mode, supplying the power to loads until the lower battery Soc limit is reached; the PV system will connected if the maximum power of battery is less than the load need or a change in the operation mode occurs (cf. Figure 7). Thus, the lower limit of the battery SoC is reached at $t \approx 2.20$ s; thereby, the PV system is connected and the BESS starts to operate in battery charging mode, as illustrated in Figures 9 and 10.

The load/generation and operation mode conditions cause undesired voltage oscillations in the dc-bus voltage, as shown in Figure 9a. For the operational conditions that are addressed in this test, the bus voltage oscillations are pretty small when the dc-bus is regulated by the proposed nonlinear robust controller, improving the time-domain transient in comparison with a classical controller. Hence, the proposed controller outperforms the classical controller, due to the minimum voltage oscillation occurrence (voltage sag and voltage swell) in the dc-bus.

5.2. Case Study II: Disconnection of the Non-Critical Load

Figures 11 and 12 show the simulation results for the case study II, where Figures 11a,b and 12a,b represent the dc-bus voltage, instantaneous powers of the dc MG, the SoC of the battery and the phase-shift control signal, and the pulse voltage of primary v_p and secondary v_s full-bridges, respectively, under different load/generation power conditions.

Like the previous case, the BESS starts operating in battery standby mode, since there is no extra power to supply or absorb from the dc MG and the battery is assumed to be fully charged.

Subsequently, two variations in the CPL power are performed from 1000-W to 1500-W and 1500-W to 3000-W, respectively (cf. Figure 11b). In this scenario, the power that loads needs (resistance load and CPL) is larger than generation power (PV system); thus, the BESS supplies the extra power to dc MG to ensure the power balance, as long as it does not exceed its maximum power or reaches the lower battery SoC limit. Hence, the BESS starts operating in battery discharging mode. For the battery discharging case, the phase-shift control signal is always positive ($\varphi > 0$), as depicted in Figure 12a; thus, the pulse voltage of the primary full-bridge (v_p) gets ahead of the pulse voltage of the secondary full-bridge (v_s), as shown in Figure 12b.

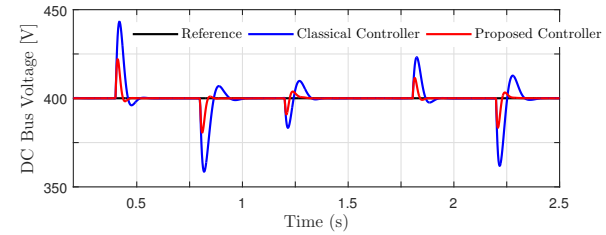

(**a**)

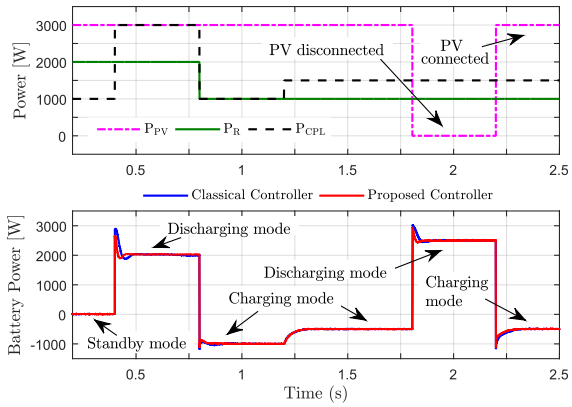

(**b**)

Figure 9. Simulated Case I: (**a**) dc–bus voltage; (**b**) microgrid power flow time–domain.

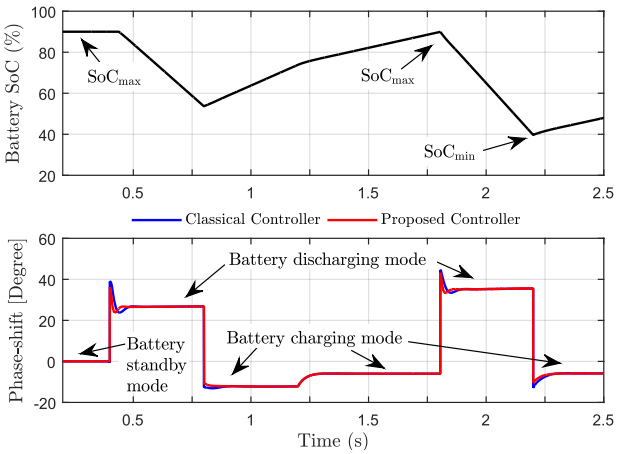

(**a**)

Figure 10. *Cont.*

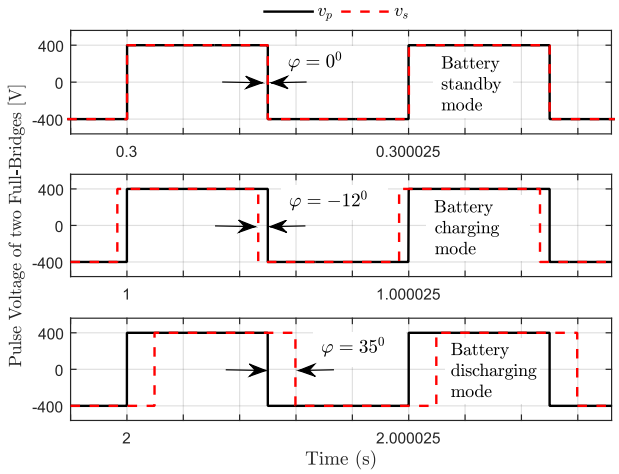

(**b**)

Figure 10. Simulated Case I: (**a**) SoC of the battery and phase–shift control; (**b**) Pulse voltage of two Full–Bridges, v_p and v_s.

After that, no load/generation variation occurs; hence, the battery will discharge until it achieves the lower battery SoC limit, resulting in a change of operation mode. If the generation power is equal to the power of loads, the power management algorithm selects the battery standby mode operation; if the power of loads is larger than the generation power, the power management algorithm will disconnect the non-critical load (CPL), and it will then select the battery charging mode operation. More details about the operation mode and power management are presented in Figure 7. In this study case, the CPL is disconnected and the battery charging mode operation is set, as shown in Figure 11b.

The BESS system will continue to operate in battery charging mode, while it does not to supply power to dc MG or the upper battery SoC limit is not reached. If the maximum charging power of battery is exceeded, then the generation power system will be disconnected and the BESS changes to battery discharging mode (cf. Figure 7).

For the battery discharging case, the phase-shift control signal is always negative ($\varphi < 0$), as depicted in Figure 12a; thus, the pulse voltage of the primary full-bridge (v_p) is lagging behind the pulse voltage of the secondary full-bridge (v_s), as shown in Figure 12b.

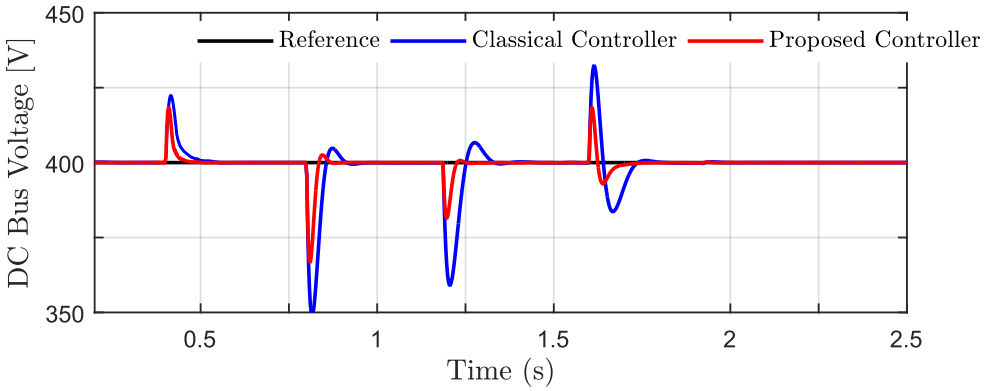

(**a**)

Figure 11. *Cont.*

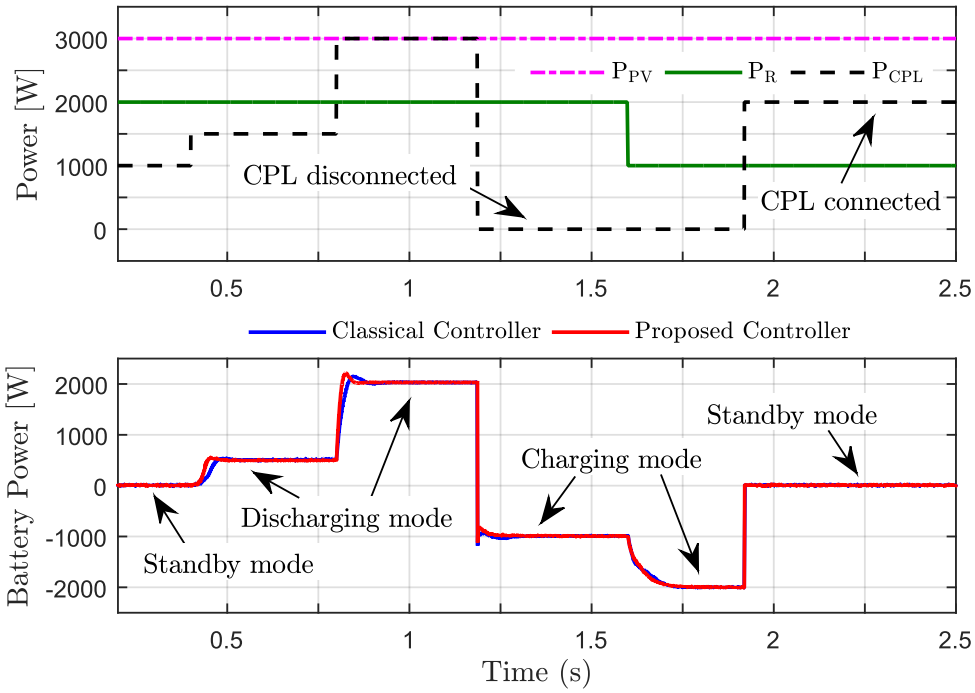

(b)

Figure 11. Simulated Case 2: (**a**) dc–bus voltage; (**b**) microgrid power flow time–domain.

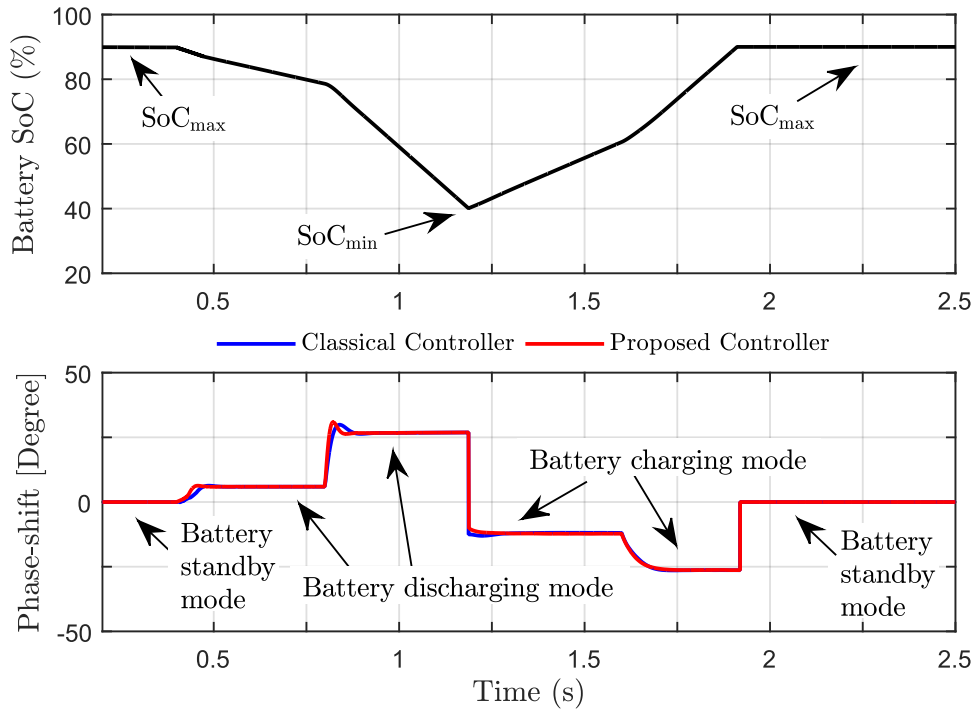

(a)

Figure 12. *Cont.*

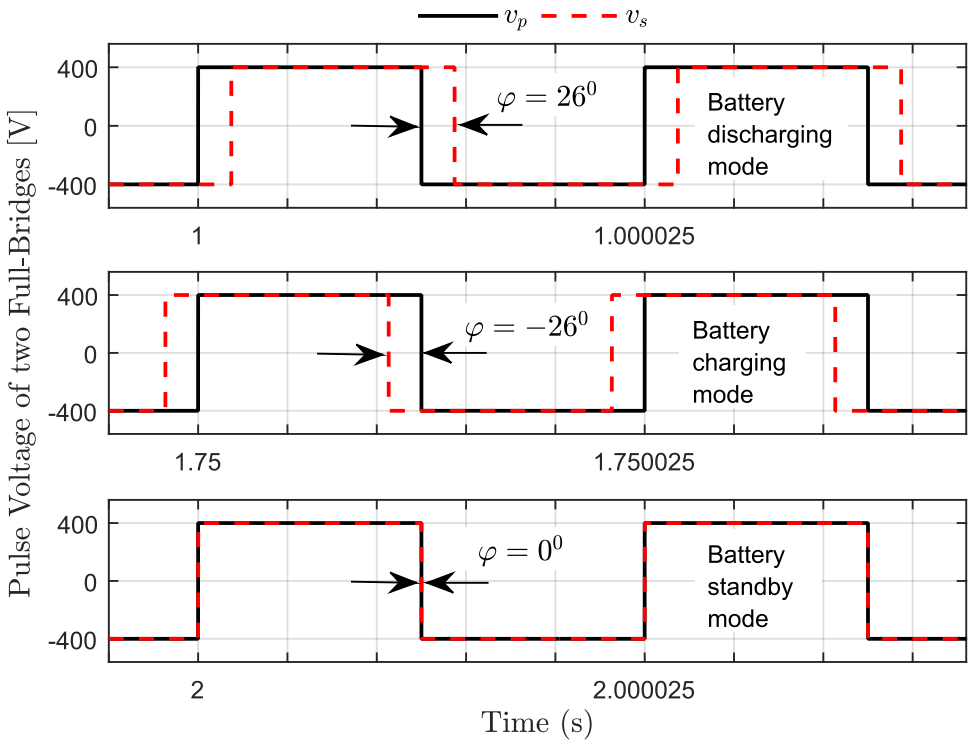

(**b**)

Figure 12. Simulated Case 2: (**a**) SoC of the battery, and phase–shift control; (**b**) Pulse voltage of two Full–Bridges, v_p and v_s.

For this case, the upper battery SoC limit is reached at $t \approx 1.85\ s$, (cf. Figure 12a); however, the PV power is larger than the power of the load resistance. In order to achieve the power balance, two scenarios are possible: (i) connect the non-critical load or (ii) disconnect the generation power system. Thereby, the CPL is connected and set the CPL power in 2500-W at this time; hence, the BESS changes to battery standby mode operation because there is no extra power to supply to the dc MG (cf. Figure 11b). Therefore, there is no phase-shift ($\varphi = 0$) between the pulse voltage of the primary (v_p) and secondary (v_s) full-bridges, as shown in Figure 12b.

Moreover, for the operational conditions that are addressed in this test, the proposed nonlinear robust controller provides better performance with reduced damping oscillation amplitude in the dc-bus voltage in comparison with a classical controller, as shown in Figure 11a. Therefore, the impact for the change in the load/generation and operation mode conditions is lower for the proposed controller.

5.3. Case Study III: DC Bus Voltage Regulation Capability

The dynamic performance of the dc-bus voltage is analyzed when the BESS operates in battery discharging mode operation in order to evaluate the effectiveness and robustness of the proposed nonlinear robust controller in comparison with a classical controller. The power management of the dc MG is ensured by the power management algorithm (cf. Figure 7).

Figure 13 shows the simulation results for the case study III. Figure 13a shows the dc-bus voltage, Figure 13b shows the instantaneous powers of the dc MG when the dc bus is regulated by the classical controller and the proposed controller, and Figure 13c shows the phase-shift control signal, and the pulse voltage of primary v_p, and secondary v_s full-bridges.

The BESS supplies the extra power to dc MG in order to ensure the power balance under different load/generation power conditions. (cf. Figure 13b). At $t = 1.0$ s, a large CPL power variation is performed from 1000-W to 3000-W. The proposed controller achieves

remaining regulation of the dc-bus voltage under this CPL power variation. However, the classical controller cannot compensate the significant oscillations in the dc-bus voltage leading to dc voltage collapse, as shown in Figure 13a. Note that φ saturates when the large CPL power variation occurs and the dc-bus is regulated by the classical controller. However, when the dc-bus is regulated by the proposed nonlinear robust controller, φ does not saturate; thus, the regulation of the dc-bus voltage remained, even under large disturbances (cf. Figure 13c).

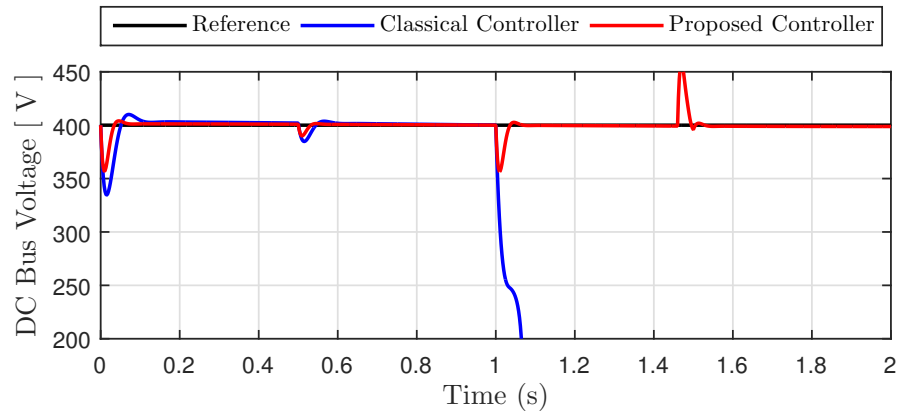

(**a**)

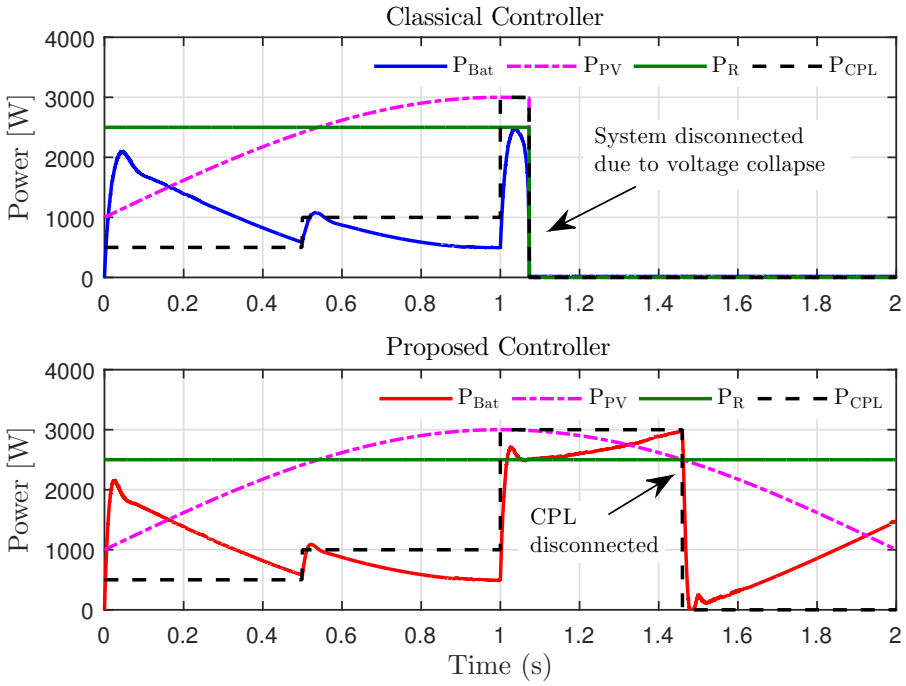

(**b**)

Figure 13. *Cont.*

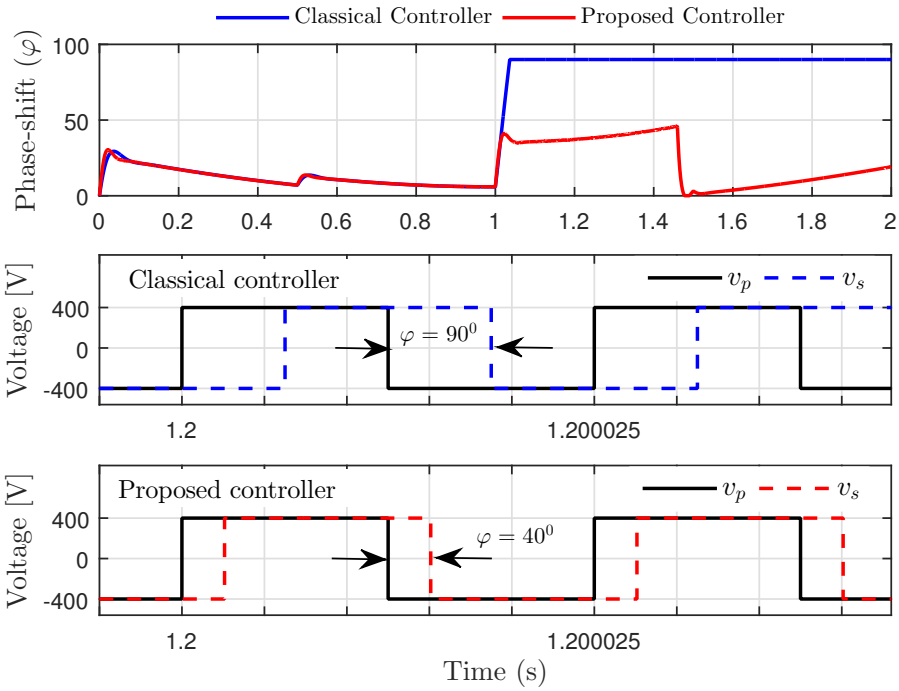

(**c**)

Figure 13. Simulated Case III: (**a**) dc–bus voltage; (**b**) microgrid power flow time–domain for classical and proposed controller; and, (**c**) phase–shift control and Pulse voltage of two Full–Bridges, v_p and v_s.

6. Conclusions

This study proposes a power management strategy for dc microgrid in stand-alone operation that includes DER (PV generation source) and BESS (battery). The dual active brigde dc-dc converter is used in order to interface the dc bus with DER and BESS. In the proposed power management strategy, the system can seamlessly switch between the battery discharging mode, battery charging mode, and battery standby mode in order to ensure the power balance in the dc microgrid under study. Moreover, since the SoC of the battery is considered in the power management algorithm, the BESS can intelligently switch its control algorithm based on its SoC and the system information (generation/load power) without the communication involved.

This paper also introduces a comprehensive view regarding the operation mode of the bidirectional DAB dc-dc converter and the operation mode of DAB converters, which interface the PV and battery storage units to ensure the power balance and regulate the dc-bus voltage in a dc microgrid. These modes of operation are handled by the proposed power management algorithm. Moreover, to enhance the robustness and reliability of the dc microgrid, we present a robust feedback linearization control approach. The proposed control technique in applied to the DAB converters of PV system and BESS when they are in voltage mode control. The proposed nonlinear robust controller ensures robust performance and stability for an entire predefined uncertainty region even under large variation in the CPL power. In addition, the proposed design method that is based on the combination of FLC and robust linear design is also an important contribution of this paper and it can be extended to other system applications that are modeled by nonlinear equations.

On the other hand, it is well-known that conventional controllers are not always adequate in order to ensure global stability and mitigate the oscillations effects of CPL and the dynamic interactions of interconnected converters. Conventional controllers only ensure system stability for small deviations of operational points. However, under large variation, the global stability cannot be ensured, because it depends on the operational region of bifurcation diagram to predict the main dynamic behaviors of the system. In this

context, a large-signal stability analysis will be addressed in the future for the proposed dc microgrid based on bifurcation analysis [7,36,39] in order to explain the global dynamic behavior of the system under study.

Author Contributions: Conceptualization, S.J.R., D.J.P. and K.E.L.; methodology, S.J.R., D.J.P. and K.E.L.; software, K.E.L.; validation, S.J.R. and K.E.L..; formal analysis, S.J.R., D.J.P. and K.E.L.; investigation, S.J.R. and K.E.L.; resources, D.J.P; data curation, D.J.P.; writing–original draft preparation, S.J.R and K.E.L.; writing–review and editing, D.J.P. and K.E.L.; visualization, S.J.R.; supervision, D.J.P. and K.E.L.; project administration, K.E.L.; funding acquisition, S.J.R. All authors have read and agreed to the published version of the manuscript.

Funding: This research was funded in part by CAPES/Brazil under Doctoral Grant Finance Code 001, in part by CNPq/BRAZIL under Project 302229/2018-3, and in part by ESPOL Polytechnic University under the R&D Project GI-GISE-FIEC-01-2018.

Conflicts of Interest: The authors declare that they have no known competing financial interests or personal relationships that could have appeared to influence the work reported in this paper.

References

1. Da Silva, R.L.; Borges, V.L.F.; Possamai, C.E.; Barbi, I. Solid-State Transformer for Power Distribution Grid Based on a Hybrid Switched-Capacitor LLC-SRC Converter: Analysis, Design and Experimentation. *IEEE Access* **2020**, *8*, 141182–141207. [CrossRef]
2. Shi, Y.; Li, R.; Xue, Y.; Li, H. Optimized Operation of Current-Fed Dual Active Bridge DC–DC Converter for PV Applications. *IEEE Trans. Ind. Electron.* **2015**, *62*, 6986–6995. [CrossRef]
3. Blinov, A.; Kosenko, R.; Vinnikov, D.; Parsa, L. Bidirectional Isolated Current Source DAB Converter with Extended ZVS/ZCS Range and Reduced Energy Circulation for Storage Applications. *IEEE Trans. Ind. Electron.* **2019**, *67*, 10552–10563. [CrossRef]
4. She, X.; Yu, X.; Wang, F.; Huang, A.Q. Design and Demonstration of a 3.6-kV–120-V/10-kVA Solid-State Transformer for Smart Grid Application. *IEEE Trans. Power Electron.* **2014**, *29*, 3982–3996. [CrossRef]
5. Iyer, V.M.; Gulur, S.; Bhattacharya, S. Small-Signal Stability Assessment and Active Stabilization of a Bidirectional Battery Charger. *IEEE Trans. Ind. Appl.* **2019**, *55*, 563–574. [CrossRef]
6. Yu, X.; She, X.; Zhou, X.; Huang, A.Q. Power Management for DC Microgrid Enabled by Solid-State Transformer. *IEEE Trans. Smart Grid* **2014**, *5*, 954–965. [CrossRef]
7. Lucas, K.E.; Pagano, D.J.; Vaca-Benavides, D.A.; García-Arcos, R.; Rocha, E.M.; Medeiros, R.L.; Ríos, S.J. Robust Control of Interconnected Power Electronic Converters to Enhance Performance in dc distribution systems: A case of study. *IEEE Trans. Power Electron.* **2020**, *36*, 4851–4863. [CrossRef]
8. Tahim, A.P.N.; Pagano, D.J.; Lenz, E.; Stramosk, V. Modeling and Stability Analysis of Islanded DC Microgrids Under Droop Control. *IEEE Trans. Power Electron.* **2015**, *30*, 4597–4607. [CrossRef]
9. Lucas-Marcillo, K.E.; Plaza Guingla, D.A.; Barra, W.; De Medeiros, R.L.P.; Rocha, E.M.; Vaca-Benavides, D.A.; Orellana, S.J.R.; Muentes, E.V.H. Novel Robust Methodology for Controller Design Aiming to Ensure DC Microgrid Stability Under CPL Power Variation. *IEEE Access* **2019**, *7*, 64206–64222. [CrossRef]
10. Shivam; Dahiya, R. Stability analysis of islanded DC microgrid for the proposed distributed control strategy with constant power loads. *Comput. Electr. Eng.* **2018**, *70*, 151–162. [CrossRef]
11. Morstyn, T.; Hredzak, B.; Agelidis, V.G. Cooperative multi-agent control of heterogeneous storage devices distributed in a dc microgrid. *IEEE Trans. Power Syst.* **2016**, *31*, 2974–2986. [CrossRef]
12. Elsayed, A.T.; Mohamed, A.A.; Mohamed, O.A. DC microgrids and distribution systems: An overview. *Electr. Power Syst. Res.* **2014**, *119*, 407–417. [CrossRef]
13. Dragičević, T.; Lu, X.; Vasquez, J.C.; Guerrero, J.M. DC Microgrids-Part I: A Review of Control Strategies and Stabilization Techniques. *IEEE Trans. Power Electron.* **2016**, *31*, 4876–4891. [CrossRef]
14. Dragičević, T.; Lu, X.; Vasquez, J.C. DC Microgrids-Part II: A Review of Power Architectures, Applications, and Standardization Issues. *IEEE Trans. Power Electron.* **2016**, *31*, 3528–3549. [CrossRef]
15. Doncker, R.W.A.A.; Divan, D.M.; Kheraluwala, M.H. A three-phase soft-switched high-power-density DC/DC converter for high-power applications. *IEEE Trans. Ind. Appl.* **1991**, *27*, 63–73. [CrossRef]
16. Zhao, B.; Song, Q.; Liu, W.; Sun, Y. Overview of Dual-Active-Bridge Isolated Bidirectional DC-DC Converter for High-Frequency-Link Power-Conversion System. *IEEE Trans. Power Electron.* **2014**, *29*, 4091–4106. [CrossRef]
17. Oggier, G.G.; GarcÍa, G.O.; Oliva, A.R. Switching Control Strategy to Minimize Dual Active Bridge Converter Losses. *IEEE Trans. Power Electron.* **2009**, *24*, 1826–1838. [CrossRef]
18. Bai, H.; Mi, C. Eliminate Reactive Power and Increase System Efficiency of Isolated Bidirectional Dual-Active-Bridge DC–DC Converters Using Novel Dual-Phase-Shift Control. *IEEE Trans. Power Electron.* **2008**, *23*, 2905–2914. [CrossRef]
19. Krismer, F.; Kolar, J.W. Closed Form Solution for Minimum Conduction Loss Modulation of DAB Converters. *IEEE Trans. Power Electron.* **2012**, *27*, 174–188. [CrossRef]

20. Fraytag, J.; Kirsten, A.L.; Heldwein, M.L. Impact analysis of a multi-variables modulation on the transformer of the dual-active-bridge converter. *IET Power Electron.* **2020**, *13*, 1041–1050. [CrossRef]
21. Hiltunen, J.; Väisänen, V.; Juntunen, R.; Silventoinen, P. Variable-Frequency Phase Shift Modulation of a Dual Active Bridge Converter. *IEEE Trans. Power Electron.* **2015**, *30*, 7138–7148. [CrossRef]
22. Costinett, D.; Maksimovic, D.; Zane, R. Design and Control for High Efficiency in High Step-Down Dual Active Bridge Converters Operating at High Switching Frequency. *IEEE Trans. Power Electron.* **2013**, *28*, 3931–3940. [CrossRef]
23. Farhangi, B.; Toliyat, H.A. Modeling and Analyzing Multiport Isolation Transformer Capacitive Components for Onboard Vehicular Power Conditioners. *IEEE Trans. Ind. Electron.* **2015**, *62*, 3134–3142. [CrossRef]
24. Fritz, N.; Rashed, M.; Bozhko, S.; Cuomo, F.; Wheeler, P. Flux control modulation for the dual active bridge DC/DC converter. *J. Eng.* **2019**, *2019*, 4353–4358. [CrossRef]
25. Lucas, K.E.; Pagano, D.J.; Medeiros, R.L.P. Single Phase-Shift Control of DAB Converter using Robust Parametric Approach. In Proceedings of the 2019 IEEE 15th Brazilian Power Electronics Conference and 5th IEEE Southern Power Electronics Conference (COBEP/SPEC), Santos, Brazil, 1–4 December 2019; pp. 1519–1524.
26. Javaid, U.; Freijedo, F.D.; Dujic, D.; van der Merwe, W. Dynamic Assessment of Source–Load Interactions in Marine MVDC Distribution. *IEEE Trans. Ind. Electron.* **2017**, *64*, 4372–4381. [CrossRef]
27. Siddique, H.A.B.; De Doncker, R.W. Evaluation of DC Collector-Grid Configurations for Large Photovoltaic Parks. *IEEE Trans. Power Deliv.* **2018**, *33*, 311–320. [CrossRef]
28. Freijedo, F.D.; Rodriguez-Diaz, E.; Dujic, D. Stable and Passive High-Power Dual Active Bridge Converters Interfacing MVDC Grids. *IEEE Trans. Ind. Electron.* **2018**, *65*, 9561–9570. [CrossRef]
29. Cupelli, M.; Gurumurthy, S.K.; Bhanderi, S.K.; Yang, Z.; Joebges, P.; Monti, A.; De Doncker, R.W. Port Controlled Hamiltonian Modeling and IDA-PBC Control of Dual Active Bridge Converters for DC Microgrids. *IEEE Trans. Ind. Electron.* **2019**, *66*, 9065–9075. [CrossRef]
30. Datta, A.J.; Ghosh, A.; Zare, F.; Rajakaruna, S. Bidirectional power sharing in an ac/dc system with a dual active bridge converter. *IET Gener. Transm. Distrib.* **2019**, *13*, 495–501. [CrossRef]
31. Tarisciotti, L.; Costabeber, A.; Chen, L.; Walker, A.; Galea, M. Current-Fed Isolated DC/DC Converter for Future Aerospace Microgrids. *IEEE Trans. Ind. Appl.* **2019**, *55*, 2823–2832. [CrossRef]
32. Vuyyuru, U.; Maiti, S.; Chakraborty, C. Active Power Flow Control Between DC Microgrids. *IEEE Trans. Smart Grid* **2019**, *10*, 5712–5723. [CrossRef]
33. Chen, L.; Gao, F.; Shen, K.; Wang, Z.; Tarisciotti, L.; Wheeler, P.; Dragicevic, T. Predictive Control based DC Microgrid Stabilization with the Dual Active Bridge Converter. *IEEE Trans. Ind. Electron.* **2020**, *67*, 8944–8956. [CrossRef]
34. Lucas Marcillo, K.E.; Guingla, D.A.P.; Barra, W.; De Medeiros, R.L.P.; Rocha, E.M.; Benavides, D.A.V.; Nogueira, F.G. Interval Robust Controller to Minimize Oscillations Effects Caused by Constant Power Load in a DC Multi-Converter Buck-Buck System. *IEEE Access* **2019**, *7*, 26324–26342. [CrossRef]
35. Bayat, H.; Yazdani, A. A Hybrid MMC-Based Photovoltaic and Battery Energy Storage System. *IEEE Power Energy Technol. Syst. J.* **2019**, *6*, 32–40. [CrossRef]
36. Tahim, A.P.N.; Pagano, D.J.; Ponce, E. Nonlinear Control of dc-dc Bidirectional Converters in Stand-alone dc Microgrids. In Proceedings of the 2012 IEEE 51st IEEE Conference on Decision and Control (CDC), Maui, HI, USA, 10–13 December 2012; pp. 3068–3073.
37. Morstyn, T.; Savkin, V.; Hredzak, B.; Agelidis, V.G. Multi-Agent Sliding Mode Control for State of Charge Balancing Between Battery Energy Storage Systems Distributed in a DC Microgrid. *IEEE Trans. Smart Grid* **2018**, *9*, 4735–4743. [CrossRef]
38. Mahmood, H.; Michaelson, D.; Jiang, J. Strategies for Independent Deployment and Autonomous Control of PV and Battery Units in Islanded Microgrids. *IEEE J. Emerg. Sel. Top. Power Electron.* **2015**, *3*, 742–755. [CrossRef]
39. Lenz, E.; Pagano, D.J.; Saito, M.T.; Pou, J. Nonlinear control of a bidirectional power converter for connecting batteries in DC microgrids. In Proceedings of the 2017 IEEE 8th International Symposium on Power Electronics for Distributed Generation Systems (PEDG), Florianopolis, Brazil, 17–20 April 2017; pp. 1–8.
40. Cai, H.; Xiang, J.; Wei, W. Decentralized Coordination Control of Multiple Photovoltaic Sources for DC Bus Voltage Regulating and Power Sharing. *IEEE Trans. Ind. Electron.* **2018**, *65*, 5601–5610. [CrossRef]
41. Cai, H.; Xiang, J.; Wei, W.; Chen, M.Z.Q. $V-dp/dv$ Droop Control for PV Sources in DC Microgrids. *IEEE Trans. Power Electron.* **2018**, *33*, 7708–7720. [CrossRef]
42. Lu, X.; Sun, K.; Guerrero, J.M.; Vasquez, J.C.; Huang, L. Double-Quadrant State-of-Charge-Based Droop Control Method for Distributed Energy Storage Systems in Autonomous DC Microgrids. *IEEE Trans. Smart Grid* **2015**, *6*, 147–157. [CrossRef]
43. Lucas, K.E.; Pagano, D.J.; Plaza, D.A.; Vaca-Benavides, D.A.; Ríos, S.J. Robust Feedback Linearization Control for DAB Converter feeding a CPL. In Proceedings of the 21st IFAC World Congress, Berlin, Germany, 12–17 July 2020; pp. 1–8.
44. Rocha, E.M.; Barra, W.; Lucas, K.E.; Medeiros, R.L.P.; Vaca-Benavides, D.A. Design and Experimental Assessment of a Robust Voltage Control for DC-DC Converters Considering Components Parametric Uncertainties. *IEEE Access* **2020**, *8*, 109217–109231. [CrossRef]